Use of Cerium Oxide Nanoparticles Conjugated with MicroRNA-146a to Correct the Diabetic Wound Healing Impairment

Carlos Zgheib, PhD, Sarah A Hilton, MD, Lindel C Dewberry, MD, Maggie M Hodges, MD, Subhadip Ghatak, PhD, Junwang Xu, PhD, Sushant Singh, PhD, Sashwati Roy, PhD, Chandan K Sen, PhD, Sudipta Seal, PhD, Kenneth W Liechty, MD, FACS, FAAP

BACKGROUND: Diabetic wounds have become one of the most challenging public health issues of the 21st century, yet there is no effective treatment available. We have previously shown that the diabetic wound healing impairment is associated with increased inflammation and decreased expression of the regulatory microRNA miR-146a. We have conjugated miR-146a to cerium oxide nanoparticles (CNP-miR146a) to target reactive oxygen species (ROS) and inflammation. This study aimed to evaluate the consequences of CNP-miR146a treatment of diabetic wounds.

STUDY DESIGN: Eight-millimeter wounds were created on the dorsal skin of Db/Db mice and treated with PBS or differing concentrations of CNP-mir146a (1; 10; 100; or 1,000 ng) at the time of wounding. Rate of wound closure was measured until the wounds were fully healed. At 4 weeks post-healing, a dumbbell-shaped skin sample was collected, with the healed wound in the center, and an Instron 5942 testing unit was used to measure the maximum load and modulus.

RESULTS: Our data showed that diabetic wounds treated with PBS or 1 ng CNP-miR146a took 18 days to heal. Treatment with 10, 100, or 1,000 ng of CNP+miR-146a effectively enhanced healing, and wounds were fully closed at day 14 post-wounding. The healed skin from the CNP-miR146a-treated group showed a trend of improved biomechanical properties (increased maximum load and modulus), however it did not reach significance.

CONCLUSIONS: We found that a 100-ng dose of CNP-miR146a improved diabetic wound healing and did not impair the biomechanical properties of the skin post-healing. This nanotechnology-based therapy is promising, and future studies are warranted to transfer this therapy to clinical application. (J Am Coll Surg 2019;228:107−115. © 2018 by the American College of Surgeons. Published by Elsevier Inc. All rights reserved.)

Diabetes has reached pandemic proportions worldwide. Complications of diabetes, such as impaired wound healing, represent a significant medical problem; the annual cost of diabetic lower extremity ulcers alone ranges from $9 billion to $13 billion, in addition to the cost for management of diabetes mellitus alone.[1,2] In addition, an ulcer of the lower extremity precedes 85% of all diabetic lower extremity amputations, and is the primary cause for hospitalization among diabetics.[3] Despite the enormous impact of these wounds on both individuals and society, effective therapies are lacking. Therefore, the modification or correction of diabetic impaired wound healing has far-reaching consequences, both on patient outcomes and on health care expenditures.

Normal wound repair follows an orderly and well-defined sequence of events that requires the interaction

Disclosure Information: Nothing to disclose.

Presented at the American College of Surgeons 104th Annual Clinical Congress, Scientific Forum, Boston, MA, October 2018.

Received July 1, 2018; Revised August 23, 2018; Accepted September 14, 2018.

From the Laboratory for Fetal and Regenerative Biology, Department of Surgery, School of Medicine, University of Colorado Denver - Anschutz Medical Campus and Colorado Children's Hospital, Aurora, CO (Zgheib, Hilton, Dewberry, Hodges, Xu, Liechty); the Department of Surgery, Comprehensive Wound Center, Ohio State University Medical Center, Columbus, OH (Ghatak, Roy, Sen); and the Advanced Materials Processing and Analysis Centre, Nanoscience Technology Center (NSTC), Materials Science and Engineering, College of Medicine, University of Central Florida, Orlando, FL (Singh, Seal).

Correspondence address: Kenneth W Liechty, MD, FACS, FAAP, University of Colorado Denver − Anschutz Medical Campus, 12700 E 19th Ave, RC2 Bldg, 6th Floor, Aurora, CO 80045. email: Kenneth.Liechty@childrenscolorado.org

https://doi.org/10.1016/j.jamcollsurg.2018.09.017
ISSN 1072-7515/18

Abbreviations and Acronyms

CNP = cerium oxide nanoparticles
Db = diabetic
IL-6 = interleukin-6
IL-8 = interleukin-8
miR-146a = microRNA-146a
NFkB = nuclear factor kappa B
ROS = reactive oxygen species
STZ = streptozocin

of many cell types and growth factors, and it is divided into inflammatory, proliferative, and remodeling phases.[4] In diabetic wounds, this complex orchestration of wound healing processes and phases are disrupted. Although the etiology is multifactorial, increased and persistent inflammation and increased oxidative stress have been implicated as central features of the wound healing impairment and complications in people with diabetes.[5-10]

The diabetic wound healing impairment and ulcer formation starts with a predisposed susceptibility for injury at baseline. We have previously shown that unwounded murine diabetic skin is biomechanically inferior when compared with skin on nondiabetic controls.[11] We found that murine diabetic skin had a much lower maximum stress and a decreased modulus of elasticity. We also showed that the biomechanical properties of diabetic skin decline during the progression of the diabetic phenotype, which increases the susceptibility of diabetic skin to injury.[9] On the other hand, we found that at 4 weeks after wounding, healed murine diabetic wounds showed no significant difference in biomechanical properties when compared with nondiabetic wounds.[11] Diabetic maximum stress and modulus were similar to those in nondiabetic samples.

Small RNA molecules or microRNA (miRNA) have been demonstrated to regulate the protein production of proinflammatory cytokines at the post-transcription level.[12,13] In particular, miR-146a has been described as one of the key regulatory molecules in the inflammatory response, acting as a "molecular brake" on the inflammatory response. MiR-146a targets and represses interleukin-1 receptor-associated kinase 1 (IRAK1) and tumor necrosis factor receptor-associated factor 6 (TRAF6). These 2 key adapter molecules of the NFkB pathway increase NFkB activity, resulting in increased expression of the genes interleukin (IL)-6 and IL-8.[14-18] We recently showed that diabetic wounds have decreased expression of miR-146a during the wound healing response.[18] We demonstrated that decreased miR-146a resulted in increased gene expression of its target genes, interleukin-1 receptor-associated kinase 1 and tumor necrosis factor receptor-associated factor 6, and a subsequent increase in NFkB signaling. Decreased expression of miR-146a in diabetic wounds may be responsible for the increased gene expression of the pro-inflammatory cytokines IL-6 and IL-8/MIP-2 and the increased inflammation seen in diabetic wounds.

Some diseases, including diabetes, have been linked to accumulation of reactive oxygen species (ROS) and their undesired effects, such as the activation of redox-sensitive transcription factors, especially NFkB.[19,20] This resulted in increased expression and production of proinflammatory cytokines such as IL-6 and IL-8, which are key mediators of inflammation. Recently, nonviral miRNA delivery strategies using nanoparticles demonstrated success. One particular type of nanoparticles present several advantages as an appropriate vehicle to deliver therapeutic miRNAs to a diabetic wound site. Cerium oxide nanoparticles (CNP) possess auto-regenerative, radical-scavenging properties due to the nanocrystalline structure of cerium oxide and the valence structure of the cerium atom caused by coexistence of 2 oxidation states reversibly switchable between 3+ and 4+ in the presence of ROS.[21-23] By scavenging the excess of ROS, these nanoparticles may be able to eliminate oxidative stress and correct the imbalance between oxidants and antioxidative enzymes in diabetic wounds.

Therefore, we propose that delivery of the anti-inflammatory miR-146a via conjugation with the antioxidative stress CNP (CNP-miR146a) decreases inflammation and oxidative stress, which will result in correction of impaired healing and improved biomechanical properties of the healed skin.

METHODS

Diabetic mouse model

All experimental protocols were approved by the Institutional Animal Care and Use Committee at University of Colorado Denver - Anschutz Medical Campus and followed the guidelines described in the NIH Guide for the Care and Use of Laboratory Animals. For all experiments, 12-week-old female mice homozygous for the Leprdb mutation (db/db) were used (BKS.Cg-Dock7m+/+Leprdb/J, strain No. 000642, Jackson Laboratory).

Cerium oxide nanoparticles synthesis and characterization

The CNP nanoparticles were synthesized using simple wet chemistry methods, as described previously.[24] In a

typical synthesis, a stoichiometric amount of cerium nitrate hexahydrate (99.999% from Sigma-Aldrich) was added to 50 mL of deionized water (18.2 MV) and stirred for 1 hour. The cerium (III) ions in the solution were oxidized to cerium (IV) oxide using excess hydrogen peroxide. After that, the pH of the solution was kept below 3.5 1 N nitric acid to maintain the synthesized ceria nanoparticles in suspension. Crystalline nanoparticles of cerium oxide form immediately on oxidation. Nanoparticles were isolated by centrifugation at 8,000 *g* for 10 minutes. Ten μM of nanoceria was prepared from 5 mM of nanoceria suspension by small aliquot dilution in pure water. Hydrodynamic size and zeta potential measurements were carried out at varying pH using dynamic light scattering measurements from Zeta Sizer Nano (Malvern Instruments), which uses a laser with wavelength at 633 nm. Different pH values in the suspension were adjusted using either ammonium hydroxide or nitric acid.

Murine wound healing model and treatment

Mice were anesthetized with inhaled isofluorane. Each mouse was shaved and depilated before wounding. The dorsal skin was swabbed with alcohol and Betadine (Purdue Pharma). Each mouse underwent a single dorsal full-thickness wound (including panniculus carnosum) with an 8-mm punch biopsy (Miltex Inc). These wounds were treated with 50 μL of PBS, 100 ng of CNP alone, 10^6 pfu of lent-imiR146a, or differing concentrations of CNP-miR146a (1; 10; 100; or 1,000 ng) at the time of wounding (Fig. 1A). All wounds were dressed with Tegaderm (3M), which was subsequently removed on postoperative day 2. Postoperatively, the mice received a subcutaneous injection of an analgesic, buprenorphine (Schering-Plough Animal Health Corp).

Murine wound area measurement

Photographs were obtained with a Nikon camera (Nikon) using a ruler for each image. ImageJ software (National Institutes of Health; http://rsbweb.nih.gov/ij/) was used to calculate the wound area of each mouse every other day. A blinded observer analyzed the size of each wound. Wound area was plotted as a function of time.

Biomechanical testing of murine skin

Biomechanical testing was performed on a full-thickness skin area from the treated mice, including the wounded area. Biomechanical testing was done 28 days post-healing on wounded skin treated with PBS or CNP-miR146a (1; 10; 100; or 1,000 ng). Skin samples immediately underwent testing after harvest; all samples had their subcutaneous tissue removed, and a uniform, dumbbell-shaped testing unit was stamped out using well-established, previously described techniques.[9,11] Cranial-caudal orientation was preserved. Two Verhoeff stain lines were placed on either end of the dumbbell shape, demarcating the gauge length of the testing area. The mean cross-sectional area of the samples tested was calculated as precisely as possible to ensure that an accurate modulus and maximum stress were calculated. The ends of the testing unit were fixed between sandpaper using a cyanoacrylate adhesive to prevent slipping. The testing unit was mounted in custom designed fixtures and tested in tension using an Instron 5543 test frame (Instron). Each testing unit underwent a previously established protocol. In short, the testing unit was preloaded to 0.005 Newtons (N), held for 120 seconds, and then subjected to a constant increase in force until the sample failed (as evidenced by tearing of the skin) and was no longer able to hold tension. Maximum stress to failure was calculated using linear regression from the linear region of the stress-strain curve. The modulus of elasticity was calculated as the slope of the stress-strain curve within the elastic region of the ramp to failure.

Swine excisional wound model and treatment

A Yorkshire white male pig was used in this study. All procedures were approved by the Ohio State University Institutional Laboratory Animal Care and Use Committee (ILACUC). To induce diabetes, the pig was injected with streptozocin (STZ) (75 mg/kg body weight) only once. To avoid hypoglycemia due to insulin released by the destroyed beta cells, 200 mL of a 5% glucose solution were given over a period of 1 hour after STZ application. Four weeks after STZ injection, the pig (47 kg) was sedated by Telazol (Butler Schein) and anesthetized by mask with isoflurane (3% to 4%). The dorsal region was shaved. The skin was surgically prepared with alternating chlorhexidine 2% and alcohol 70% (Butler Schein) scrubs. Under such aseptic conditions, 2 sets of 5 full-thickness excisional wounds (1"×1") were established on the back of pigs with a depth of approximate 2 cm, to reach the subcutaneous fat in all wounds. A total of 5 wounds were created on each side of the back. A scaled plastic template was used to create the wounds at fixed distance from each other and from the spine (4 cm), starting below the lower border of the scapula on the dorsum of the pig. Wounds from 1 side of the back were treated with a CNP-miR146a (100 ng) followed by dressing with Tegaderm, while the wounds from the contralateral side of the back were dressed with Tegaderm only and received only PBS (control). Digital photographs were taken on days 0, 3, 7, 10, and 14 for measurement of the wound area. The pig was maintained on 12-hour light—dark cycles and was euthanized 14 days post-wounding.

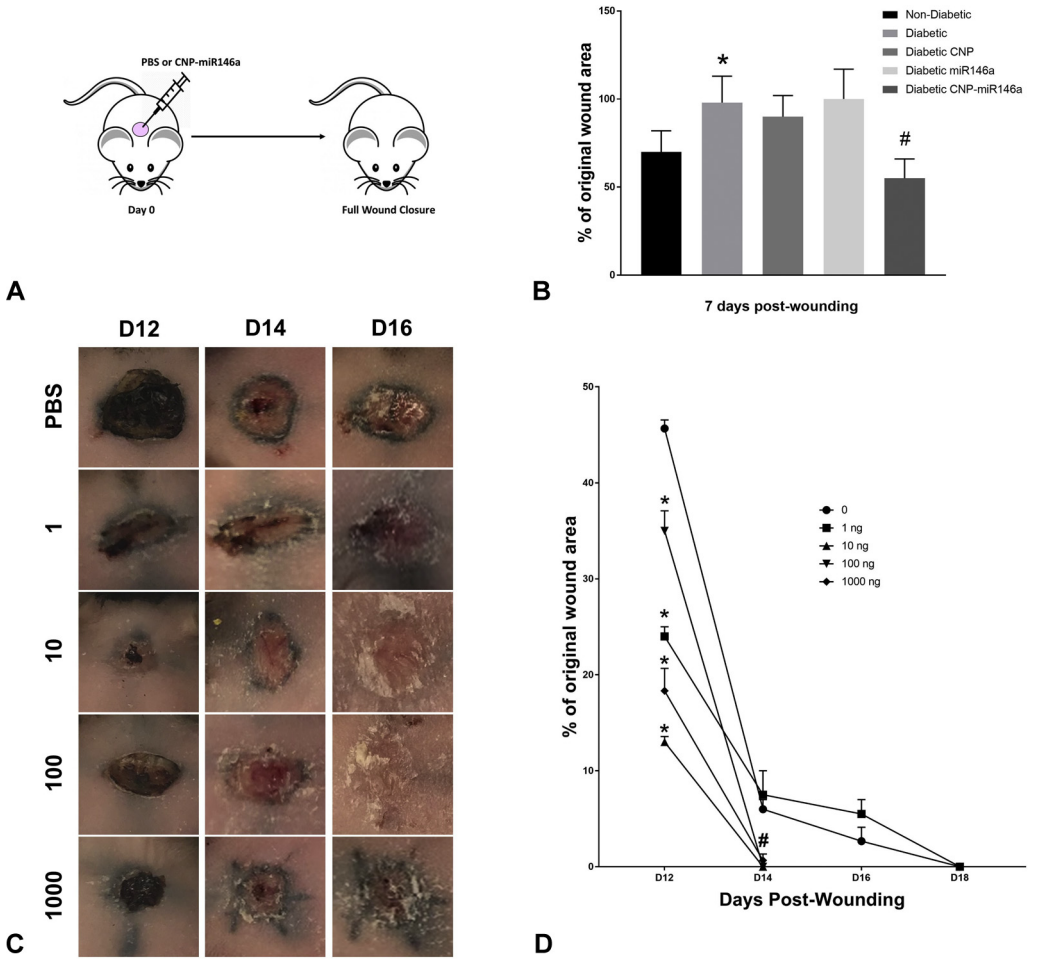

Figure 1. Cerium oxide nanoparticles (CNP)-miR146a improve diabetic wound healing. (A) Graphic representation of the wounding protocol and treatment in the diabetic mouse. (B) Graphic representation of nondiabetic wounds (PBS), diabetic wounds (PBS), and diabetic wounds treated with 100 ng CNP, 10^6 PFU LentimiR-146a, or 100 ng of CNP-miR146a at day 7 post-wounding. *$p < 0.05$ compared with nondiabetic wounds and #$p<0.05$ compared with diabetic wounds by Student's *t*-test. (C) Representative photographs (days 12, 14, and 16 post-wounding) of diabetic murine wounds treated with 0 (PBS), 1, 10, 100, or 1,000 ng of CNP-miR146a at the time of wounding. (D) Graphic representation of wound closure timeline in diabetic wounds treated with 0 (PBS), 1, 10, 100, or 1,000 ng of CNP-miR146a at the time of wounding. n = 3 per group; *$p < 0.05$ comparing 0 to 1 ng, 0 to 10 ng, 0 to 100 ng, or 0 to 1,000 ng; # $p < 0.05$ comparing 0 or 1 ng to 10, 100, or 1,000 ng by Student's *t*-test.

All wounds were digitally photographed in the presence of a standard reference ruler. Wound area was calculated using the ImageJ software. The pig was maintained on standard chow ad libitum, fasted overnight before the procedures, and housed individually in the animal facility. The pig was maintained on 12-hour light—dark cycles and was euthanized after the completion of experiments.

Swine wounds histologic analysis

At day 14 post-wounding, the animal was euthanized and the wound-edge tissue (2 cm from the edge) was collected in formalin from the control (PBS) and treated (1,300 ng CNP-miR146a). Five-micron microtomed sections were placed on positive charged slides. Some slides underwent Masson's Trichrome staining. The rest of the slides were deparaffinized. Once sections were hydrated they were placed in citrate buffer pH 6.0, and heat-induced epitope retrieval was performed using the Biocare Medical's Decloaker. The slides were then stained using Leica's Bond Rx instrument, and all reagents were applied robotically onto slides. The slides were incubated with primary CD45 and CD31 antibodies (BD Biosciences) at 1:50 dilutions. They were developed with a Vectastain Elite ABC kit with secondary antibody (Vector Laboratories). A blinded observer analyzed the numbers of CD31-positive and CD45-positive cells per high-power field.

Statistical analysis

The *t*-test was used to analyze the data. All data were expressed as the mean ± SEM and a value of $p < 0.05$ was considered significant.

RESULTS

Treatment of diabetic wounds with CNP-miR146a accelerates healing

Figure 1B shows the percentage of original wound area at day 7 post-wounding for nondiabetic wounds (PBS), diabetic wounds (PBS), and diabetic wounds treated with 100 ng CNP, 10^6 PFU LentimiR-146a, or 100 ng of CNP-miR146a. The percentage of open wounds among diabetic wounds is significantly higher than in nondiabetic wounds at day 7 post-wounding. Treatment with 100 ng of CNP-miR146a significantly enhances diabetic wound healing. On the other hand, CNP or miR-146a alone did not improve healing. Treatment of diabetic wounds with the CNP-miR146a resulted in a significant improvement of wound healing. Diabetic wounds treated with PBS (0 ng) were significantly larger at days 14 and 16 compared to diabetic wounds treated with CNP-miR146a (Fig. 1C). Our data showed that diabetic wounds treated with PBS or 1 ng CNP-miR146a took 18 days to heal. Treatment with 10, 100, or 1,000 ng of CNP+miR-146a effectively enhanced the rate of wound closure, and wounds were fully closed at day 14 post-wounding (Fig. 1D).

Diabetic skin maintained its biomechanical properties post-healing

At 4 weeks after wounding, healed murine diabetic wounds treated with (1, 10, or 100 ng) CNP-miR146a showed a trend toward improved biomechanical properties compared with the PBS-treated wounds; however, it did not reach significance (Fig. 2A). The average modulus for the healed skin treated with PBS was 11.09 ± 5.98 MPa (Fig. 2B). For the healed skin treated with 1, 10, 100, and 1,000 ng of CNP-miR146a, the average modulus was 13.5 MPa, 13.71 MPa, 12.6, and 8.5 MPa, respectively (Fig. 2B).

Diabetic skin did not develop any pathologic abnormalities after treatment

Histopathologic microscopic examination of skin samples from mice treated with PBS or different doses of CNP-miR146a did not reveal any pathology or lesions (Fig. 3). In addition, no soft tissue abnormalities were noted in the majority of tissues; multiple soft tissues were microscopically reviewed, there was excess adipose tissue, but nothing appeared abnormal for this strain of diabetic mouse.

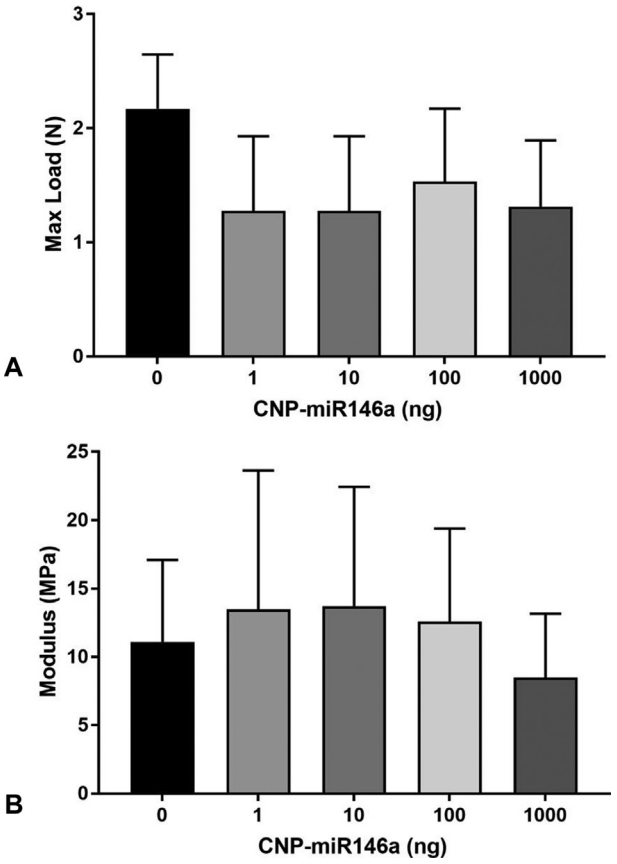

Figure 2. Cerium oxide nanoparticles (CNP)-miR146a maintained the biomechanical properties of diabetic skin post-healing. Figure 2A displays the maximum load and 2B displays the modulus of skin samples collected at day 28 post-healing from wounds treated with 0 (PBS), 1, 10, 100, or 1,000 ng of CNP-miR146a at the time of wounding. Student's *t*-test showed no significant difference between the treatment groups.

CNP-miR146a improves healing in a clinically relevant model of diabetes

To induce diabetes, the pig was injected with STZ (75mg/kg body weight) only once, as shown in Figure 4A. Wounds were created at 1 month post-STZ injection. Five of 10 wounds on the right side were treated with CNP-miR146a at day 0, as shown in Figure 4B. Digital imaging of the wounds was performed on days 0, 3, 7, 10, and 14 for measurement of wound area. Figure 4C shows representative digital photographs of 2 wounds at day 14, 1 treated with PBS and another with CNP-miR146a. These photographs show that at day 14 post-wounding, the wound treated with CNP-miR146a is clearly smaller in size compared with the wound treated with PBS.

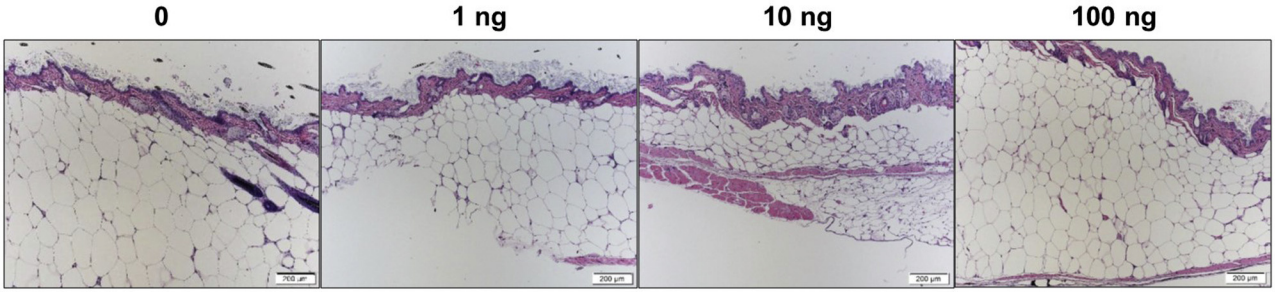

Figure 3. Cerium oxide nanoparticles (CNP)-miR146a did not induce any pathologic abnormalities in the diabetic skin post-healing. Histopathologic microscopic examination of skin samples from diabetic wounds treated with 0 (PBS), 1, 10, 100 ng of CNP-miR146a at day 28 post-healing.

Figure 4D shows graphic analysis of the areas of all 10 wounds, measured by digital planimetry. At day 10, the PBS-treated wounds had an average surface area of 6.8 $cm^2 \pm 0.46$; the surface area of the CNP-miR146a treated wounds was 4.8 $cm^2 \pm 0.24$. By day 14, the average surface areas of the PBS and CNP-miR146a treated wounds were 4.63 $cm^2 \pm 0.21$ and 3.06 $cm^2 \pm 0.28$, respectively (Data expressed as mean $\pm$ SEM, $^*p < 0.05$).

CNP-miR146a decreases inflammation and increases angiogenesis in diabetic wounds

The effect of CNP-miR146a treatment on inflammation was assessed using immunohistochemistry for CD45, the common leukocyte antigen. Representative photos of immunoperoxidase staining for CD45 at 14 days in swine diabetic wounds treated with PBS or CNP-miR146a are demonstrated in Figure 5A. Quantitative analysis of diabetic wounds treated with CNP-miR146a demonstrated a significant decrease in CD45-positive cells compared with PBS-treated diabetic wounds (Fig. 5B).

The effect of CNP-miR146a treatment on angiogenesis was assessed using immunohistochemistry for endothelial marker CD31. Representative photos of immunoperoxidase staining for CD31 at 14 days in swine diabetic wounds treated with PBS or CNP-miR146a are shown in Figure 5A. Quantitative analysis of diabetic wounds treated with CNP-miR146a demonstrated a significant increase in the number of vessels compared with PBS-treated diabetic wounds (Fig. 5B).

The effect of the CNP-miR146a on fibrosis was assessed at 14 days using trichrome staining. Representative sections from both PBS- and CNP-miR146a-treated wounds are displayed in Figure 5. Treatment with CNP-miR146a did not result in a significant change in fibrosis compared with the PBS-treated diabetic wounds.

DISCUSSION

This study demonstrates the potential of a novel therapeutic agent for diabetic wounds, CNP-miR146a. Local treatment of the diabetic wound with CNP or miR146a alone did not have an effect on the rate of wound closure in diabetic wounds; however; treatment with CNP-miR146a conjugate resulted in reduced time to wound healing, with increased strength and elasticity in a murine model (Figs. 1 and 2). This was further validated in a porcine model in which treatment with CNP-miR146a resulted in reduced time to wound healing, with associated decreased inflammation and increased angiogenesis (Figs. 4 and 5). No adverse effects from treatment with CNP-miR146a were seen in the murine or porcine model (Fig. 3). These findings are promising for the clinical application of this nanoparticle therapeutic in the challenging area of diabetic wound healing.

Previous studies have demonstrated the important role of miR-146a in decreasing pathologic inflammation in the diabetic wound and have shown that the treatment of diabetic wounds with mesenchymal stem cells increased miR-146a expression.[18] However, application of mesenchymal stem cells as a therapeutic remains challenging, highlighting the need for a different delivery mechanism, such as conjugated nanoparticles. In another murine wounding model, application of cerium oxide nanoparticles has demonstrated accelerating wound healing through proliferation of fibroblasts, keratinocytes, and vascular endothelial cells.[23] This is likely related to the ROS scavenging properties of cerium oxide nanoparticles as well as modulation of the intracellular oxygen environment.[25,26] Therefore, combining these properties of cerium oxide nanoparticles with the anti-inflammatory properties of miR-146a, as in our study, results in decreased inflammation, increased angiogenesis, and improved wound healing.

Wound healing progresses through inflammatory, proliferative, and remodeling phases. In diabetic wounds,

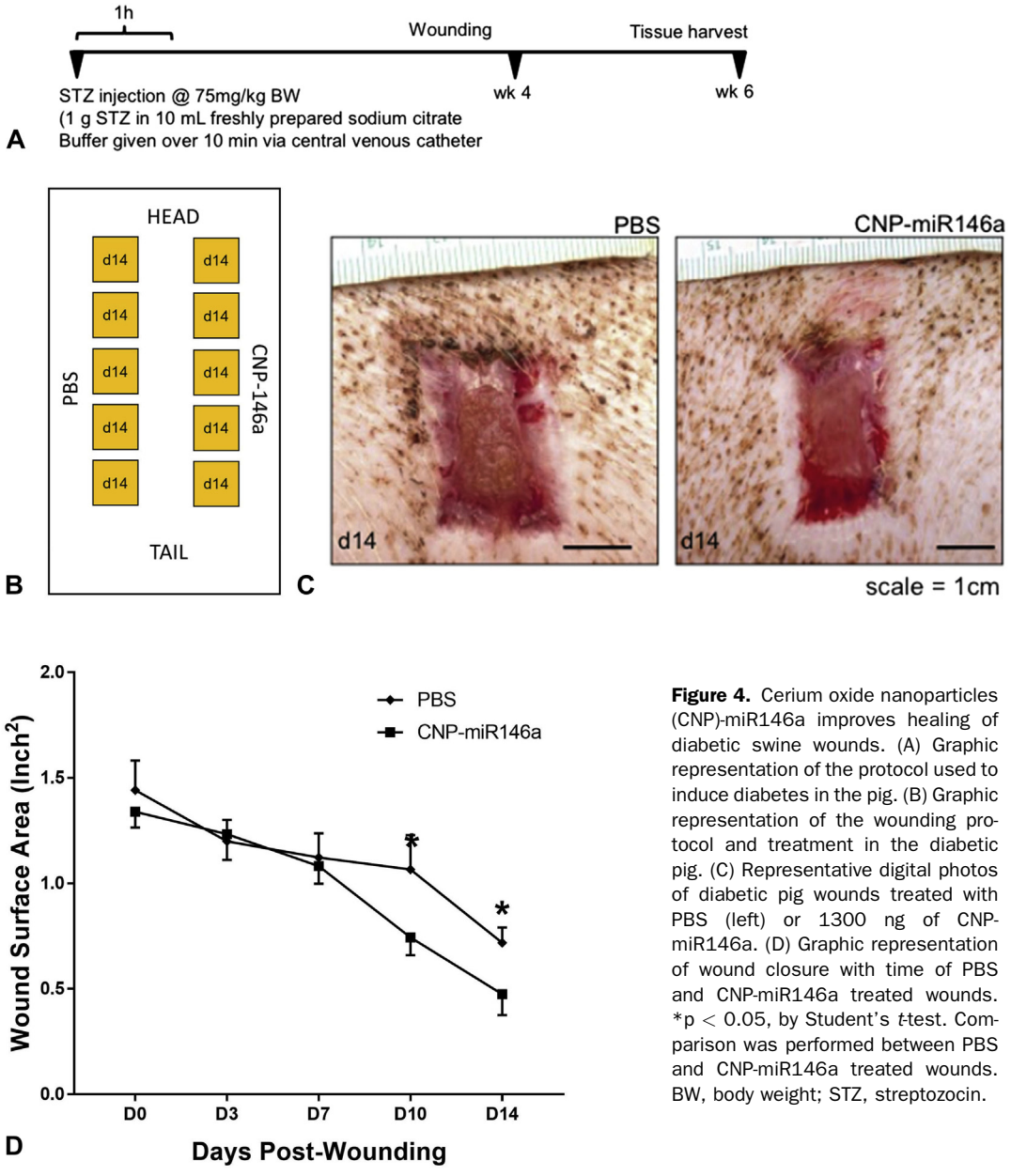

Figure 4. Cerium oxide nanoparticles (CNP)-miR146a improves healing of diabetic swine wounds. (A) Graphic representation of the protocol used to induce diabetes in the pig. (B) Graphic representation of the wounding protocol and treatment in the diabetic pig. (C) Representative digital photos of diabetic pig wounds treated with PBS (left) or 1300 ng of CNP-miR146a. (D) Graphic representation of wound closure with time of PBS and CNP-miR146a treated wounds. *$p < 0.05$, by Student's *t*-test. Comparison was performed between PBS and CNP-miR146a treated wounds. BW, body weight; STZ, streptozocin.

these phases are dysregulated with a prolonged inflammatory phase. Treatment with CNP-miR146a decreases the inflammation in the wound and allows the wound to progress to the proliferative and remodeling phase (Fig. 5). This is supported by our study; the porcine model not only demonstrates a statistically significant improved rate of wound closure in the treatment group, but also, improved granulation tissue and wound appearance of CNP-miR146a group at 14 days (Fig. 4). Furthermore, there is evidence to suggest dysregulation in the proliferative and remodeling phases as well, with diabetic skin demonstrating decreased collagen I levels and collagen I:III ratios compared with normal skin. This is associated with decreased strength and elasticity on evaluation with biomechanical testing.[9,11] Our study suggests that this inherent dysregulation of proliferation and remodeling, with resulting decreased strength and elasticity, may be corrected with CNP-miR146a treatment, but further testing is needed. Compared with other therapeutics on the market that decrease time to wound healing,

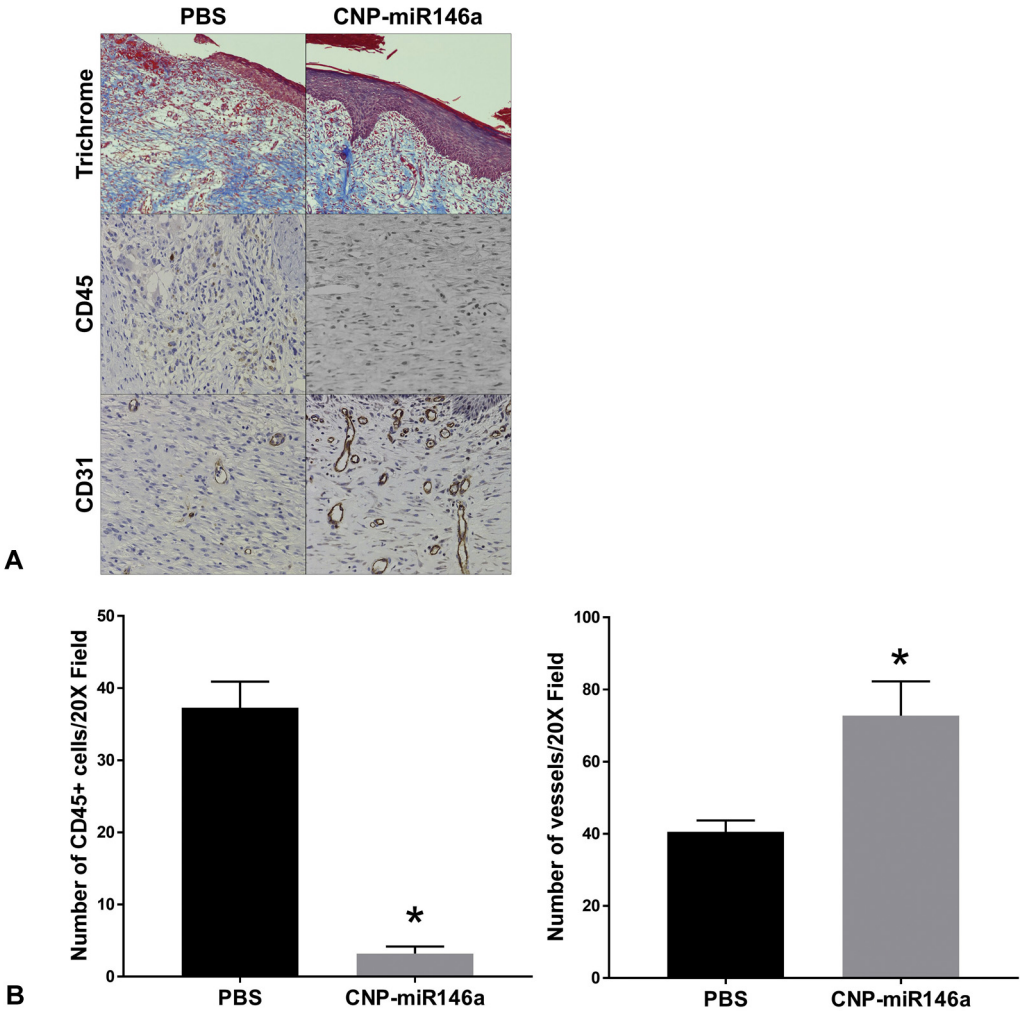

Figure 5. Cerium oxide nanoparticles (CNP)-miR146a-treated wounds showed similar fibrosis levels, decreased inflammation, and increased angiogenesis. (A) Masson's trichrome, CD45+, and CD31+ staining of representative sections of diabetic swine wounds after 14 days of treatment with treated with PBS (n = 5) or CNP-miR146a (n = 5). (B) Quantitative analysis of number of CD45 positive cells and number of vessels (CD31 staining) per 20× field. *$p < 0.05$, by Student's *t*-test. Comparison was performed between PBS and CNP-miR146a treated wounds.

such as platelet-derived growth factor, CNP-MiR146a has the ability to improve both time to wound closure and ultimate skin strength.[27]

A strength of this study includes the use of a porcine wounding model in addition to a murine model. Porcine skin better represents wound healing seen in humans with regard to granulation tissue and epithelialization, providing a more clinically relevant model than mice. The persistent hyperglycemia induced in pigs leads to delayed epithelialization and impaired wound healing, similar to that in human diabetic wounds.

Diabetic mice are a well-established model for dysfunctional wound healing, but this model is limited due to the contracture that occurs in mice during healing. Other authors have used devices to prevent wound contracture in mice, but this model still does not account for granulation seen in human wound healing. Therefore, we chose to move further study to the porcine model. Diabetic mice are a well-established model for dysfunctional wound healing, but this model is limited due to the contracture that occurs in mice during healing. Other authors have used devices to prevent wound contracture in mice, but this model still does not account for granulation seen in human wound healing. Therefore, we chose to move further study to the porcine model. The porcine model is limited due to the acute nature of induced diabetes and a lack of long-term diabetic sequela.

CONCLUSIONS

In conclusion, CNP-miR146a improves wound healing in a murine and porcine diabetic wound model without compromising wound strength or elasticity. Future directions include validation in human clinical trials.

Author Contributions

Study conception and design: Zgheib, Hilton, Roy, Sen, Seal, Liechty

Acquisition of data: Zgheib, Hilton, Dewberry, Hodges, Ghatak

Analysis and interpretation of data: Zgheib, Hilton, Dewberry, Hodges, Ghatak, Xu, Singh, Roy, Sen, Seal, Liechty

Drafting of manuscript: Zgheib, Hilton, Dewberry, Hodges, Ghatak, Xu, Singh, Roy, Sen, Seal, Liechty

Critical revision: Zgheib, Hilton, Roy, Sen, Seal, Liechty

Acknowledgment: We would like to thank Professor Linda K Johnson DVM, MS, MPH, Director of the Comparative Pathology Shared Resource (CPSR), Department of Pathology, UC Denver, Anschutz Medical Campus, for her help with the pathology analysis.

REFERENCES

1. Ragnarson Tennvall G, Apelqvist J. Health-economic consequences of diabetic foot lesions. Clin Infect Dis 2004;39[Suppl 2]:S132–S139.
2. Rice JB, Desai U, Cummings AK, et al. Burden of diabetic foot ulcers for Medicare and private insurers. Diabetes Care 2014;37:651–658.
3. Boulton AJ, Vileikyte L, Ragnarson-Tennvall G, et al. The global burden of diabetic foot disease. Lancet 2005;366:1719–1724.
4. Lepäntalo M, Apelqvist J, Setacci C, et al. Chapter V: Diabetic foot. Eur J Vasc Endovasc Surg 2011;42[Suppl 2]:S60–S74.
5. Eming SA, Martin P, Tomic-Canic M. Wound repair and regeneration: mechanisms, signaling, and translation. Sci Transl Med 2014;6:265sr6.
6. Khanna S, Biswas S, Shang Y, et al. Macrophage dysfunction impairs resolution of inflammation in the wounds of diabetic mice. PLoS One 2010;5:e9539.
7. Dhall S, Do DC, Garcia M, et al. Generating and reversing chronic wounds in diabetic mice by manipulating wound redox parameters. J Diabetes Res 2014;2014:562625.
8. Zgheib C, Xu J, Liechty KW. Targeting inflammatory cytokines and extracellular matrix composition to promote wound regeneration. Adv Wound Care (New Rochelle) 2014;3:344–355.
9. Zgheib C, Hodges M, Hu J, et al. Mechanisms of mesenchymal stem cell correction of the impaired biomechanical properties of diabetic skin: The role of miR-29a. Wound Repair Regen 2016;24:237–246.
10. Zgheib C, Liechty KW. Shedding light on miR-26a: Another key regulator of angiogenesis in diabetic wound healing. J Mol Cell Cardiol 2016;92:203–205.
11. Bermudez DM, Herdrich BJ, Xu J, et al. Impaired biomechanical properties of diabetic skin implications in pathogenesis of diabetic wound complications. Am J Pathol 2011;178:2215–2223.
12. Moura J, Børsheim E, Carvalho E. The role of microRNAs in diabetic complications-special emphasis on wound healing. Genes (Basel) 2014;5:926–956.
13. Mulholland EJ, Dunne N, McCarthy HO. MicroRNA as therapeutic targets for chronic wound healing. Molec Ther Nucleic Acids 2017;8:46–55.
14. Xie Y, Chu A, Feng Y, et al. MicroRNA-146a: A comprehensive indicator of inflammation and oxidative stress status induced in the brain of chronic T2DM rats. Front Pharmacol 2018;9:478.
15. Feng Y, Chen L, Luo Q, et al. Involvement of microRNA-146a in diabetic peripheral neuropathy through the regulation of inflammation. Drug Des Devel Ther 2018;12:171–177.
16. Lo WY, Peng CT, Wang HJ. MicroRNA-146a-5p mediates high glucose-induced endothelial inflammation via targeting interleukin-1 receptor-associated kinase 1 expression. Front Physiol 2017;8:551.
17. Bhatt K, Lanting LL, Jia Y, et al. Anti-inflammatory role of microRNA-146a in the pathogenesis of diabetic nephropathy. J Am Soc Nephrol 2016;27:2277–2288.
18. Xu J, Wu W, Zhang L, et al. The role of microRNA-146a in the pathogenesis of the diabetic wound-healing impairment: correction with mesenchymal stem cell treatment. Diabetes 2012;61:2906–2912.
19. Wei W, Liu Q, Tan Y, et al. Oxidative stress, diabetes, and diabetic complications. Hemoglobin 2009;33:370–377.
20. Zgheib C, Hodges MM, Hu J, et al. Long non-coding RNA Lethe regulates hyperglycemia-induced reactive oxygen species production in macrophages. PLoS One 2017;12:e0177453.
21. Walkey C, Das S, Seal S, et al. Catalytic properties and biomedical applications of cerium oxide nanoparticles. Environ Sci Nano 2015;2:33–53.
22. Das S, Dowding JM, Klump KE, et al. Cerium oxide nanoparticles: applications and prospects in nanomedicine. Nanomedicine (Lond) 2013;8:1483–1508.
23. Chigurupati S, Mughal MR, Okun E, et al. Effects of cerium oxide nanoparticles on the growth of keratinocytes, fibroblasts and vascular endothelial cells in cutaneous wound healing. Biomaterials 2013;34:2194–2201.
24. Karakoti AS, Monteiro-Riviere NA, Aggarwal R, et al. Nanoceria as antioxidant: synthesis and biomedical applications. JOM (1989) 2008;60:33–37.
25. Korsvik C, Patil S, Seal S, et al. Superoxide dismutase mimetic properties exhibited by vacancy engineered ceria nanoparticles. Chem Commun (Camb) 2007;10:1056–1058.
26. Das S, Singh S, Dowding JM, et al. The induction of angiogenesis by cerium oxide nanoparticles through the modulation of oxygen in intracellular environments. Biomaterials 2012;33:7746–7755.
27. Wieman TJ, Smiell JM, Su Y. Efficacy and safety of a topical gel formulation of recombinant human platelet-derived growth factor-BB (becaplermin) in patients with chronic neuropathic diabetic ulcers. A phase III randomized placebo-controlled double-blind study. Diabetes Care 1998;21:822–827.